Comparative Analysis of Three-Winding High-Frequency Transformer Parameter Estimation Methodologies

Giuseppe Bossi
Department of Electrical and Electronic Engineering
University of Cagliari
Cagliari, Italy
giuseppe.bossi@unica.it

Ali Arshad
Department of Electrical and Electronic Engineering
University of Cagliari
Cagliari, Italy
ali.arshad@unica.it

Alfonso Damiano
Department of Electrical and Electronic Engineering
University of Cagliari
Cagliari, Italy
alfonso.damiano@unica.it

***Abstract*—This paper presents a methodology for the full characterisation of a three-winding high-frequency transformer. The proposed approach is based on short-circuit and open-circuit tests, also using an impedance analyser to determine its electrical and magnetic parameters. The transformer under study is a prototype manufactured by the SIRIO company for on-board chargers of electric vehicles. In order to evaluate the proposed methodology, a comparative analysis has been carried out with several existing strategies reported in the literature. Finally, the effectiveness of the proposed modelling of a three-winding high-frequency transformer was validated by comparing the co-simulation study using MATLAB and PLECS with experimental results.**

***Index Terms*—Electric vehicles, on-board chargers, high-frequency transformer, impedance measurement, characterization.**

I. Introduction

High-frequency transformers play a crucial role in integrated on-board chargers (OBC) of electric vehicles (EVs). Typically, the power electronics of OBC use two separate two-winding isolation transformers to interface high-voltage and low-voltage batteries, separately [1], [9]. However, the use of three-winding high-frequency transformer (3W-HFT) can reduce the size, weight, and cost of EV chargers while simultaneously improving the system efficiency and power quality [2]. Nevertheless, the implementation of 3W-HFT introduces design challenges, particularly in transformer modeling and characterization. In this context, transformer leakage inductances play an important role, especially when topologies such as the triple-active bridge (TAB) are employed, because leakage inductance significantly influences power flow. Therefore, the development of an effective 3W-HFT model is essential to optimize its design and improve conversion efficiency, for example, by achieving zero-voltage switching (ZVS) operation [2]–[4], [11]–[13]. Various analytical approaches have been proposed in the literature, primarily focusing on leakage inductance evaluation. The π-model has been selected as the preferred modeling technique for the three-winding transformer [2], [4]–[10].

In high-frequency applications, the electrostatic parasitic components of a 3W-HFT significantly influence the system response specifically during switching. To account for these effects, the parasitic capacitances are represented in the π-model. This modeling approach is often preferred due to its high accuracy and simplicity, particularly for designing isolated three-port converters [5], [6].

Previous studies in the transformer modeling have primarily focused on power flow analysis, leakage inductance effects, and decoupling strategies in three-port systems [2], [6]–[8]. However, these models did not fully consider transformer parasitic effects, leading to discrepancies between expected and actual system performance at high frequencies.

This paper proposes a complete methodology for the characterization of a three-winding high-frequency transformer, which effectiveness is validated throughout comparative analysis with four other strategies. The organization of this paper is as follows: Section II presents the modeling and the characterization strategies of the 3W-HFT; Section III reports the co-simulation and experimental validation that demonstrate the effectiveness of the proposed methodology. Finally, Section IV concludes the paper by summarizing the key findings.

II. Characterization of the Three-Winding High-Frequency Transformer

A. Modeling of the Transformer

The proposed transformer model is depicted in Fig. 1. It consists of the primary port (P) and two secondary ports (S_1 and S_2), characterized by the turn ratios N_{S_1} and N_{S_2}, respectively. The magnetization impedance is represented by the iron resistance R_{fe} and the magnetization inductance L_m, both referenced to the primary side.

This study was carried out within the MOST - Sustainable Mobility National Research Center and received funding from the European Union NextGenerationEU (National Recovery and Resilience Plan (NRRP) - MISSION 4 COMPONENT2, INVESTMENT 1.4 - D.D. 1033 17/06/2022, CN00000023).

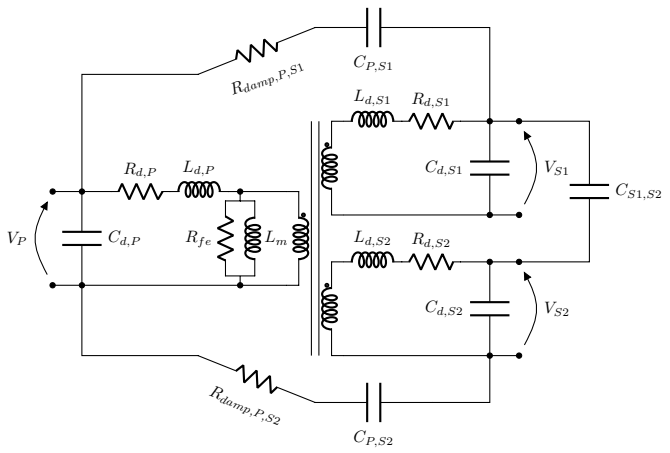

Fig. 1. Proposed π-model of the three-winding high-frequency transformer.

Each winding is modeled with its respective leakage inductance L_d ($L_{d,P}$, L_{d,S_1}, and L_{d,S_2}) and conduction resistance R_d ($R_{d,P}$, R_{d,S_1}, and R_{d,S_2}), to account for magnetic and electric losses, respectively. Moreover, each port presents a stray capacitance C_d ($C_{d,P}$, C_{d,S_1}, and C_{d,S_2}) and the inter-winding capacitances C_{P,S_1}, C_{P,S_2}, and C_{S_1,S_2}, linking each transformer port.

B. Proposed Transformer Parameter Estimation Method

The proposed methodology concerns to evaluate the magnetizing inductance by measuring the magnetization current and to measure the parasitics with an impedance analyzer. In particular, the impedance analyzer Keysight E9440A has been employed, and it is shown in Fig. 2. This instrument allows for precise measurements in a frequency range between 20 Hz and 50 MHz. To ensure the precision and reliability of the measurements, the Keysight E9440A impedance analyzer was calibrated before testing using open/short/load compensation.

The proposed methodology comprises three experimental measurements. Firstly, an open-circuit test is conducted on the transformer using a laboratory setup for measuring the magnetization current. A square wave voltage is applied to the primary winding through an H-bridge converter, and the corresponding voltage and current waveforms are recorded using an oscilloscope. The voltage and the rate of change of the current $\frac{di}{dt}$ were acquired and magnetization inductance L_m is evaluated resorting to (1).

$$V = L_m \frac{di}{dt} \tag{1}$$

Subsequently, the open-circuit impedance variation over a wide frequency range has then been determined by means of an impedance analyser. The first resonance frequency f_0 that occurs while sweeping the frequencies is consider to evaluate the iron resistance and the stray capacitances. In particular, the impedance value assumed at f_0, Z_{oc,f_0}, is considered the iron resistance R_{fe}, while the stray capacitances C_d are directly evaluated from the inductance value at f_0, L_0, by solving (2).

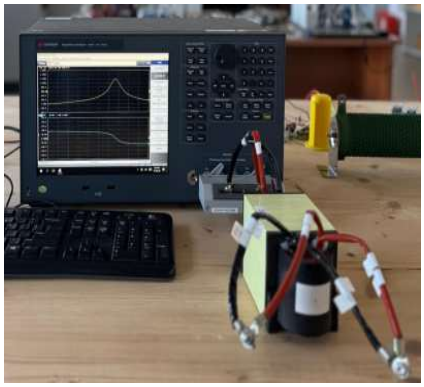

Fig. 2. Keysight E9440A to perform measurements from 20Hz up to 13MHz.

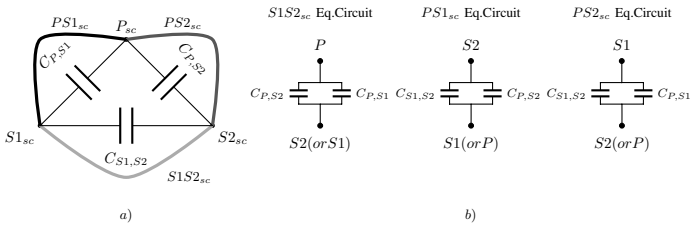

Fig. 3. *Capacitance measurement setup for the three-winding transformer. (a) Setup for measuring $C_{P,S1}$, $C_{P,S2}$, and $C_{S1,S2}$; (b) Interwinding capacitance measurement configuration.*

$$f_0 = \frac{1}{2\pi\sqrt{L_0 C_d}} \tag{2}$$

Afterwards, a the short-circuit impedance vs frequency has been determined resorting to impedance analyser. Inductance and resistance measurements evaluate the equivalent short-circuit inductance L_{sc} and resistance R_{sc} of each transformer port. By solving the system reported in (3), $L_{d,P}$, $L_{d,S1}$, and $L_{d,S2}$ are evaluated, where the superscripts $'$, $''$, and $'''$ indicate the parameters reflected on P, $S1$, and $S2$, respectively. In the same way, a similar system allows one to identify $R_{d,P}$, $R_{d,S1}$, or $R_{d,S2}$.

$$\begin{cases} L'_{d,P} + \dfrac{L'_{d,S_1} L'_{d,S_2}}{L'_{d,S_1} + L'_{d,S_2}} = L'_{sc}, \\ L'_{d,S_1} + \dfrac{L'_{d,P} L'_{d,S_2}}{L'_{d,P} + L'_{d,S_2}} = \dfrac{L''_{sc}}{N_{S_1}}, \\ L'_{d,S_2} + \dfrac{L'_{d,P} L'_{d,S_1}}{L'_{d,P} + L'_{d,S_1}} = \dfrac{L'''_{sc}}{N_{S_2}}. \end{cases} \tag{3}$$

The inter-winding capacitances are determined by short-circuiting each winding separately, forming the nodes P_{sc}, S_{1sc}, and S_{2sc}, as shown in Fig. 3a.

By short-circuiting two transformer nodes at a time, the parallel combination of the inter-winding capacitances is determined, as shown in Fig. 3b. Thus, each capacitance is evaluated according to (4).

$$\begin{cases} C_{P,S1} + C_{P,S2} = C_{S1S2_{sc}} \\ C_{P,S2} + C_{S1,S2} = C_{PS1_{sc}} \\ C_{P,S1} + C_{S1,S2} = C_{PS2_{sc}} \end{cases} \tag{4}$$

Finally, the damping resistances R_{damp,PS_1} and R_{damp,PS_2} are determined by identifying the resonance frequencies f_1 and f_2. These frequencies are obtained by short-circuiting one of the ports while keeping the others open-circuited, from which the damping resistance is evaluated.

For example, if R_{damp,PS_1} needs to be determined, the measurement is taken from P, while S_1 is short-circuited and S_2 is open-circuited. In this way, the impedance Z_{sc,f_1} is evaluated, which corresponds to R_{damp,PS_1}.

C. Existing Transformer Parameter Estimation Methods

Several methodologies have been considered for comparison:

- **Strategy A** is based on inductance measurements from the terminal analysis described in [6];
- **Strategy B** involves calculating the magnetization inductance separately, and the leakage inductance values are determined by the open-circuit equations [2], [7], [8].
- **Strategy C** use the one-port impedance measurement method [2]. This strategy includes magnetization inductance in the short-circuit equation model to achieve more accurate parameter calculations.
- **Strategy D** represent an alternative inductance evaluation approach proposed in [7]. This strategy modifies the model equations from Strategy-A by adjusting the referred inductance.

The transformer model employed in these methodologies is depicted in Fig. 4. This model provides a structured representation of self and mutual inductances, enabling the direct computation of leakage and magnetizing inductances using the inductance matrix, making it particularly advantageous for inductance estimation. These methodologies are widely used in power electronics and transformer design to analyze power flow, leakage inductance effects, and decoupling strategies in three-port systems. The leakage inductance estimation in Strategies A and B was determined using equations derived from open-circuit tests, as represented in (5).

$$\begin{cases} L_{\sigma 1} = L_{11} - \frac{M_{12}M_{13}}{M_{23}}, \\ L_{\sigma 2} = L_{22} - \frac{M_{12}M_{23}}{M_{13}}, \\ L_{\sigma 3} = L_{33} - \frac{M_{23}M_{13}}{M_{12}}, \\ M_0 = \frac{M_{12}M_{13}}{M_{23}}. \end{cases} \tag{5}$$

This system of equations relies on mutual inductances (M_{12}, M_{13}, M_{23}), which are highly sensitive to core nonlinearity, parasitic effects, and measurement inaccuracies. Even small errors in these values can propagate through calculations, leading to numerical instability in leakage inductance estimation. This issue is further exacerbated when large self-inductance values are subtracted to obtain small leakage inductance values, often resulting in negative inductance values, making the estimation unreliable. Additionally, parasitic capacitances and resistances can introduce further inaccuracies by affecting impedance measurements, further compromising the precision of the results.

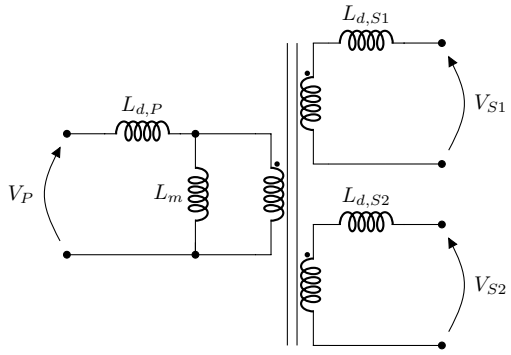

Fig. 4. π-model of the three-winding transformer.

Nevertheless, Strategies A and C employed short-circuit test equations as reported in (6), leading to improved precision and consistency in leakage inductance estimation. This short-circuit-based approach effectively captures leakage flux while minimizing the reliance on sensitive mutual inductance values. By directly measuring inductances, it reduces numerical instability and external influences, offering a more reliable approach for three-winding transformers.

$$\begin{cases} L_{11} = \frac{1}{2}(L_{12} + L_{13} - L'_{23}), \\ L'_{22} = \frac{1}{2}(L_{12} + L'_{23} - L_{13}), \\ L'_{33} = \frac{1}{2}(L_{13} + L'_{23} - L_{12}). \end{cases} \tag{6}$$

Referring to the methodology proposed in this work, the dual-port shorting method of (3) offers a more precise estimation of leakage inductance by simultaneously capturing interactions between two windings. Unlike the single-port shorting method, which relies on sequential measurements and is susceptible to error propagation, this approach minimizes dependence on mutual inductance calculations, reducing measurement noise. Additionally, it requires fewer tests to determine all essential transformer parameters, enhancing its applicability in both simulations and hardware implementations. Furthermore, this method provides a more accurate representation of the dynamic interactions among multiple windings, aligning closely with real-world transformer behaviour.

III. Simulation and Experimental Results

The transformer parametrization methodologies has been applied to a 3W-HFT prototype, manufactured by the SIRIO company. This transformer have two output ports with turn ratios of 1:0.5 and 1:0.25, corresponding to S_1 and S_2, respectively. The rated power is 20 kW, distributed as 10 kW on each output port, and the rated voltage is 700 V.

TABLE I
HALF-BRIDGE MODULE RATING

Parameter	Symbol	Value	Unit
DC Rated Voltage	U_{DC}	800	V
DC Maximum Continuous Current	I_{DC}^{max}	24	A_{RMS}
DC Maximum Pulsed Current	I_{DC}^{pulsed}	80	A
Reference Switching Frequency	f_{sw}	20	kHz
DC Side Bus Capacitance	C_{DC}	260	μF

TABLE II
SIC MOSFET ELECTRICAL CHARACTERISTICS

Parameter	Symbol	Value	Unit
Drain-Source Voltage	U_{ds}	1200	V
Continuous Drain Current	I_D^{SiC}	24	A
Power Dissipation	P_D^{SiC}	192	W
Reference Switching Frequency	f_{sw}	20	kHz
Drain-Source On-State Resistance	R_{ds}^{on}	128	mΩ
Turn-On Switching Energy	E_{on}^{sw}	265	μJ
Turn-Off Switching Energy	E_{off}^{sw}	135	μJ

The parameters evaluated applying the proposed model are reported in Table III. Moreover, Table III reports the leakage inductances evaluated using the strategies A, B, C, and D. As can be noted, strategies B and D yielded negative parameters, making them unsuitable for the transformer under study. This results can be ascribed to their reliance on idealized mutual inductance distributions and impedance matrix formulations, which do not distinguish mutual inductance contributions from short-circuit resistance. These limitations rendered them unsuitable for the transformer under study. Conversely, Strategy-A and Strategy-C produced non-negative leakage inductance values, demonstrating a reliable estimation approach.

The experimental test for determining the magnetization current considers a square-wave voltage of 400 V at 20 kHz. In this context, a square-wave voltage is preferred over a sinusoidal waveform since the constant voltage peaks generate a linear magnetizing current ramp, simplifying the evaluation of the magnetizing inductance. The square-wave voltage is generated using an H-bridge circuit equipped silicon carbide (SiC) MOSFETs, which main characteristics are reported in Table I and Table II, respectively. The SiC MOSFETs are widely recognized for their high efficiency and fast switching capabilities, enabling an accurate assessment of the transformer performance. The experimental setup is reported in Fig. 5. Figs. 6 and 7 illustrate the acquired experimental results, obtained directly from the oscilloscope, showing the voltages and current. As expected, the magnetizing current exhibits a triangular waveform, where the ramps correspond to the constant peak voltage and magnetization inductance is evaluated resorting to (1).

A co-simulation study using MATLAB and PLECS was conducted, with results compared against experimental data.

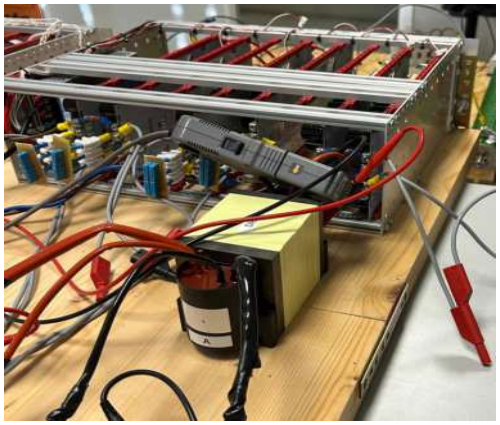

Fig. 5. Experimental setup of H-bridge utilized silicon carbide (SiC) MOSFETs.

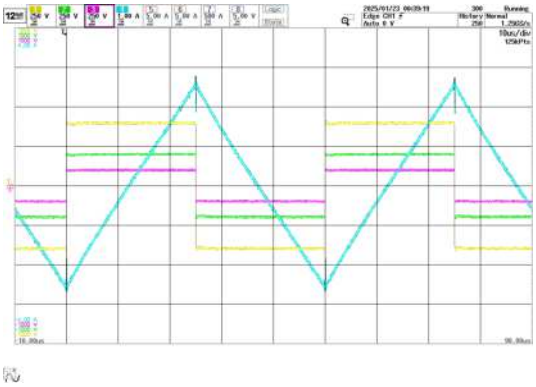

Fig. 6. Measured voltage and current waveforms during transformer testing.

In Figs. 8 and 9, a comparison is presented between the simulation and the experimental results obtained using the proposed strategy, demonstrating a strong alignment between both results, particularly concerning stray capacitance effects. These effects cause a distortion corresponding to the peak of the triangular wave.

In Figs. 10, 11, 12, and 13, a comparison is made between the simulation results of strategies A and C and the corresponding experimental results. The observed differences between the experimental peak current and the simulated values highlight certain deviations, indicating the influence of real-world factors on the transformer performance.

The stronger correlation between simulation and experimental results confirms the accuracy and reliability of the proposed methodology, particularly due to the modeling of the parasitic capacitive behaviour. These findings contribute to advancing transformer modeling techniques, which are crucial for optimizing the design and performance evaluation of high-frequency power converters.

IV. CONCLUSION

This paper presents a complete methodology for the characterization of a three-winding high-frequency transformer, incorporating both short-circuit and open-circuit tests to ac-

TABLE III
PARAMETERS OF THE THREE-WINDING HIGH-FREQUENCY TRANSFORMER

Parameter	Proposed Strategy	Strategy A	Strategy B	Strategy C			Strategy D
$L_{d,P}$ (μH)	3.1	3.2	-24	1700	3.2	14000	7.7
L_{d,S_1} (μH)	0.72	0.76	-1300	1.3	0.77	24000	-0.35
L_{d,S_2} (μH)	0.41	0.55	-1600	0.32	0.54	5900	0.27
L_m (mH)	2.00	1.7	1.7	-500	1.7	-12	1.7
$R_{d,P}$ $(m\Omega)$	20	–	–	–	–	–	–
R_{d,S_1} $(m\Omega)$	14	–	–	–	–	–	–
R_{d,S_2} $(m\Omega)$	5.6	–	–	–	–	–	–
R_m $(k\Omega)$	150	–	–	–	–	–	–
$C_{d,P}$ (μF)	58.6	–	–	–	–	–	–
C_{d,S_1} (μF)	247	–	–	–	–	–	–
C_{d,S_2} (μF)	960	–	–	–	–	–	–
C_{P,S_1} (μF)	269	–	–	–	–	–	–
C_{P,S_2} (μF)	288	–	–	–	–	–	–
C_{S_1,S_2} (μF)	275	–	–	–	–	–	–
R_{damp,PS_1} $(k\Omega)$	1.99	–	–	–	–	–	–
R_{damp,PS_2} (Ω)	3.14	–	–	–	–	–	–

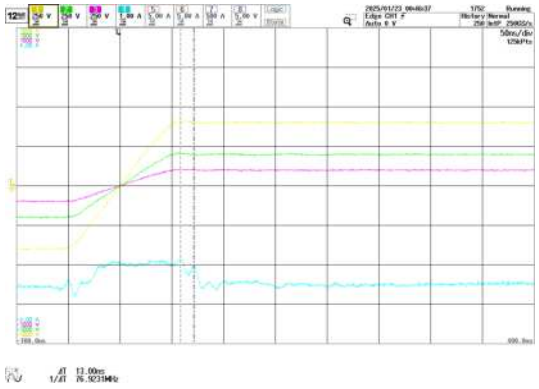

Fig. 7. Transient response of voltage and current waveforms during switching interval.

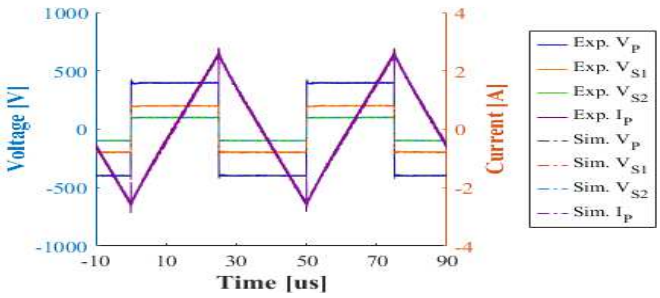

Fig. 8. Comparison between experimental and simulated result for transformer voltage and current Waveforms of proposed strategy.

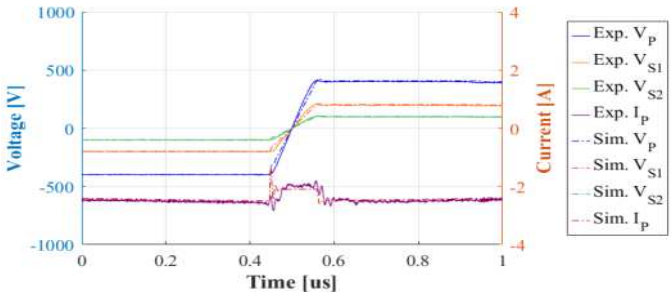

Fig. 9. Comparison between experimental and simulated result for transformer waveforms at switching interval of proposed strategy.

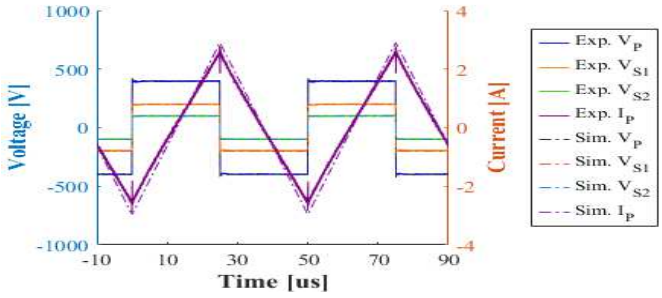

Fig. 10. Comparison between experimental and simulated result for transformer voltage and current Waveforms of strategy-A.

curately determine its electrical and magnetic parameters. A comparative analysis was conducted against four existing parameter estimation methodologies from the literature to evaluate their effectiveness. a co-simulation and experimental results validate the proposed characterization methodology and in the comparison analysis demonstrates batter performances with respect to other methodologies, particularly concerning the electrostatic effects.

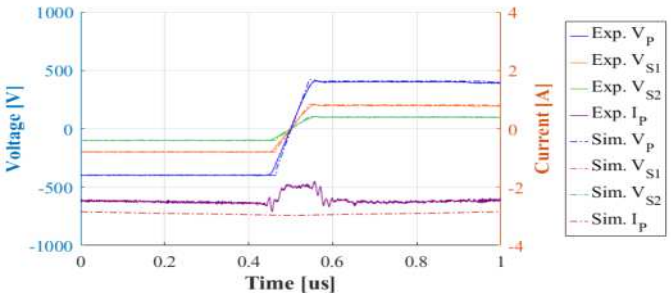

Fig. 11. Comparison between experimental and simulated result for transformer waveforms at switching interval of strategy-A.

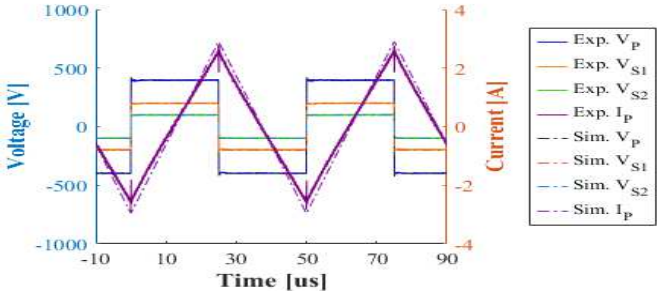

Fig. 12. Comparison between experimental and simulated result for transformer voltage and current Waveforms of strategy-C.

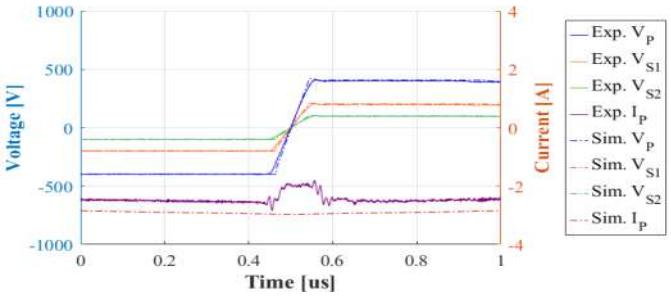

Fig. 13. Comparison between experimental and simulated result for transformer waveforms at switching interval of strategy-C.

ACKNOWLEDGMENT

This study was carried out within the MOST - Sustainable Mobility National Research Center and received funding from the European Union Next-GenerationEU (National Recovery and Resilience Plan (NRRP) - MISSION 4 COMPONENT2, INVESTMENT 1.4 - D.D. 1033 17/06/2022, CN00000023) The authors wish to thank the staff of "Piattaforma Energie Rinnovabili"- Sardegna Ricerche for their active support and specifically Dr. Malgorzata Gawronska and Dr. Carla Sanna.

REFERENCES

[1] G. Yu and S. Choi, "An Effective Integration of APM and OBC With Simultaneous Operation and Entire ZVS Range for Electric Vehicle," *IEEE Transactions on Power Electronics*, vol. 36, no. 9, pp. 10343-10354, 2021.

[2] I. Kougioulis, A. Vannini, A. Pal, P. Wheeler and M. R. Ahmed, "Estimation of Leakage Inductance in High-frequency Three-Winding Transformers for Electric Vehicle On-board Chargers," in *Proc. 25th European Conf. Power Electronics and Applications (EPE'23 ECCE Europe)*, Aalborg, Denmark, 2023.

[3] P. Purgat, S. Bandyopadhyay, Z. Qin and P. Bauer, "Zero Voltage Switching Criteria of Triple Active Bridge Converter," *IEEE Transactions on Power Electronics*, vol. 36, no. 5, pp. 5425-5439, May 2021.

[4] D. I. Zaikin, "Comparison of Three-Winding Transformer Model Extraction Using FEMM and COMSOL Multiphysics®," in *Proc. 21st Int. Conf. Mechatronics - Mechatronika (ME)*, Brno, Czech Republic, 2024.

[5] K. I. Hwu and Y. H. Chen, "Estimation of individual leakage inductances of a transformer based on measurements," in *Proc. IEEE Int. Conf. Industrial Technology*, Chengdu, China, 2008.

[6] S. S. Chakraborty, S. Dey and K. Hatua, "Design of a Three-Winding Transformer for Power Decoupling of a Three-Port Series Resonant Converter for an Integrated On-Board EV Charger," *IEEE Transactions on Power Electronics*, vol. 38, no. 11, pp. 14262-14273, Nov. 2023.

[7] S. Deb and S. K. Pramanick, "Investigation of Leakage Inductance in Three-Winding Transformer for Three-Port Integrated Onboard Chargers," in *Proc. IEEE Transportation Electrification Conf. and Expo (ITEC)*, Chicago, IL, USA, 2024.

[8] J. G. Hayes, N. O'Donovan and M. G. Egan, "The extended T model of the multiwinding transformer," in *Proc. IEEE 35th Annu. Power Electronics Specialists Conf. (PESC)*, Aachen, Germany, 2004.

[9] M. D. Alam, M. M. Rahman, I. Husain, and S. Lukic, "Circulating power and winding current minimization in a triple active bridge DC-DC converter with optimized leakage inductance design," in *Proc. IEEE Appl. Power Electron. Conf. Expo. (APEC)*, Long Beach, CA, USA, 2024, pp. 474–480, doi: 10.1109/APEC48139.2024.10509037.

[10] F. de Leon and J. A. Martinez, "Dual three-winding transformer equivalent circuit matching leakage measurements," *IEEE Trans. Power Del.*, vol. 24, no. 1, pp. 160–168, Jan. 2009, doi: 10.1109/TPWRD.2008.2007012.

[11] B. Rahrovi, R. T. Mehrjardi, and M. Ehsani, "On the analysis and design of high-frequency transformers for dual and triple active bridge converters in more electric aircraft," in *Proc. IEEE Texas Power Energy Conf. (TPEC)*, College Station, TX, USA, 2021, pp. 1–6, doi: 10.1109/TPEC51183.2021.9384990.

[12] R. Chattopadhyay, G. Gohil, and S. Bhattacharya, "Split-winding type three-limb core structured HF transformer for integrating PV and energy storage (ES)," in *Proc. IEEE Appl. Power Electron. Conf. Expo. (APEC)*, Tampa, FL, USA, Mar. 2017, pp. 2997–3004, doi: 10.1109/APEC.2017.7931186.

[13] M. Jafari, M. R. Islam, Z. Malekjamshidi, and J. Zhu, "Modeling of multi-winding high-frequency transformers as a common magnetic-link in smart micro-grids," in *Proc. Int. Conf. Electr. Electron. Eng. (ICEEE)*, Rajshahi, Bangladesh, 2015, pp. 249–252, doi: 10.1109/CEEE.2015.7428269.